


Double-well Bose-Hubbard model with nearest-neighbor and cavity-mediated long-range interactions

Johannes Sicks* and Heiko Rieger

Theoretical Physics, Saarland University, Campus E2.6, 66123 Saarbrücken, Germany

 (Received 1 October 2023; revised 5 February 2024; accepted 13 February 2024; published 22 March 2024)

We consider a one-dimensional Bose-Hubbard model (BHM) with on-site double-well potentials and study the effect of nearest-neighbor repulsion and cavity-mediated long-range interactions by calculating the ground-state phase diagrams with quantum Monte Carlo simulations. We show that when the intrawell repulsion is as strong as the on-site repulsion, a dimerized Mott-insulator phase appears at the tip of the dimerized density-wave phase for a density of one particle per double well. Furthermore, we find a dimerized Haldane-insulator phase in the double-well BHM with nearest-neighbor interaction, which is identical to a dimerized BHM with repulsive interactions up to the third neighbor.

DOI: [10.1103/PhysRevA.109.033317](https://doi.org/10.1103/PhysRevA.109.033317)

I. INTRODUCTION

Since its introduction, the Bose-Hubbard model (BHM) [1] has been a focus of research. In the simplest form, where tunneling between neighboring sites and a repulsive on-site interaction exist, the ground-state phase diagram is characterized by two phases. For commensurate fillings and large on-site repulsions compared to the bosonic tunneling, a Mott-insulator (MI) phase appears, while for incommensurate fillings or weak on-site repulsion, the superfluid (SF) phase exists.

Jaksch *et al.* showed [2] that the dynamics of ultracold bosons, which are contained by an optical lattice, realize a BHM. This was experimentally shown by Greiner *et al.* [3] and led, consequentially, to a broad study of experiments of ultracold bosons in optical lattices [4–8].

The universality class of the SF-MI phase transition in the BHM is generally of mean-field type, except for the multicritical point, where particle-hole symmetry holds [1]. At this point, the universality class changes to the type of the $(d + 1)$ -dimensional XY model [9–11], where the two-dimensional XY model [12,13] has a topological Kosterlitz-Thouless phase transition [14,15]. Furthermore, when the occupation per site is restricted to zero, one, and two bosons per site, the one-dimensional BHM can be described by a quantum spin-1 chain, which features a gapped Haldane-insulator phase, characterized by a nonlocal order parameter [16–20].

The quantum critical phenomena of the BHM were studied extensively with quantum Monte Carlo (QMC) methods, like the path-integral [21,22], world-line [23,24], and worm-algorithm QMC [25,26], of which we use the latter in this work. Also, approximate methods were used, like the mean-field theory [1,27] and density-matrix renormalization-group method [28].

There are many different modifications and extensions to the BHM, originating from the addition of interactions or changes to the confining potentials. Possible interactions

are the nearest-neighbor interaction [28–35] (also referred to as extended BHM), next-nearest-neighbor interaction [16,36] and hopping [37], cavity-mediated long-range interaction [4,38–40], and combinations of nearest-neighbor and long-range interaction [41,42]. Changes to the confining potentials include, for instance, disordered potentials [43,44] and double-well potentials [45–51].

Two superimposed optical lattices with different wavelengths form a so-called superlattice, like the double-well lattice, in which each site consists of a double-well potential [45,52]. With the help of double-well lattices, quantum information processes can be studied [53,54] because they allow, for example, to manipulate atoms individually [55] or study the many-body dynamics and entanglement of a double-well chain [48]. Furthermore, the hard-core double-well BHM is the bosonic counterpart of the Su-Schrieffer-Heeger model [56] for free fermions, which possesses a nontrivial topological insulator phase. For the hard-core double-well BHM, this topological phase was shown as well [51,57], and the ground-state properties were studied recently [58].

In this paper, we study the ground-state phase diagram of the one-dimensional extended double-well BHM with cavity-mediated long-range interaction. In this model, each lattice site consists of one double-well potential, and these potentials are aligned in a chain. We consider nearest-neighbor interaction between the sites; therefore, bosons in both wells of the double well on one site feel the interactions between all wells of the neighboring double-well sites. Also, the intrawell repulsion between the two wells of each double well is taken into account.

The model's parameter space includes a one-dimensional extended single-well BHM with long-range interaction, where additional density-wave (DW), supersolid (SS), and Haldane-insulator (HI) phases appear [42], and a one-dimensional dimerized BHM, where intrawell repulsion and hopping strength alternate between every other site [7,58–62] and bond-ordered phases appear [63].

Open questions that we will address in this paper include (1) the dependence of the existence of the bond-ordered (dimerized) phase on the particle density, (2) the differences

*johannes@lusi.uni-sb.de

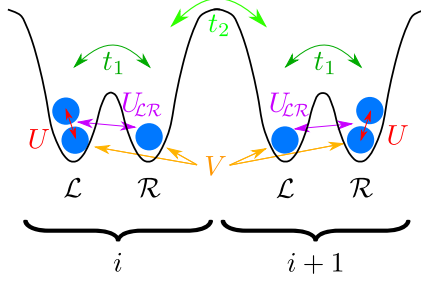


FIG. 1. Sketch of two sites of the double-well Bose-Hubbard model according to the interactions in Hamiltonian (1) without the \hat{H}_{U_d} term. Each site consists of a double well with a left (\mathcal{L}) and a right (\mathcal{R}) well. In each well, bosons experience an on-site repulsion U when two or more bosons are present. Intrawell tunneling t_1 is possible between the left and right wells of the same site, and interwell tunneling t_2 is possible between the left and right wells of adjacent sites. Intrawell repulsion $U_{\mathcal{L}\mathcal{R}}$ is present between the left and right wells of the same site, and the nearest-neighbor interaction V interacts between all wells of adjacent sites.

between strong and weak intrawell potentials, and (3) the effect of cavity-mediated long-range interactions on the phase diagram of the double-well BHM.

This paper is organized as follows: In Sec. II, the Hamiltonian of the one-dimensional extended double-well BHM with cavity-mediated long-range interaction is defined, and the order parameters are introduced. Then, a description of the occurring phases is given, and the analytically solvable ground states without hopping terms are discussed. Section III contains the QMC worm-algorithm results for the ground states of the standard and extended double-well BHMs. First, we examine the standard double-well BHM, before giving results for the extended double-well BHM and double-well BHM with cavity-mediated long-range interaction. The conclusions are given in Sec. IV.

II. MODEL

A. Hamiltonian of the double-well BHM

We state the one-dimensional extended double-well BHM Hamiltonian with cavity-mediated long-range interaction. In Fig. 1 we depict all interactions of the Hamiltonian except for the cavity-mediated long-range interaction. Each site position contains one double well and is labeled by the index $i \in 1, \dots, L$, while the left and right wells of the respective double well are given by $\sigma \in \{\mathcal{L}, \mathcal{R}\}$. Here, L is the length of the chain. We use periodic boundary conditions; thus, $L + 1, \sigma \equiv 1, \sigma$.

The Hamiltonian operator for the one-dimensional extended double-well BHM with cavity-mediated long-range interaction reads

$$\hat{H} = \hat{H}_t + \hat{H}_U + \hat{H}_{U_{\mathcal{L}\mathcal{R}}} + \hat{H}_V + \hat{H}_\mu + \hat{H}_{U_d}, \quad (1)$$

where the particular terms have the following forms.

\hat{H}_t denotes the hopping terms,

$$\hat{H}_t = -t_1 \sum_i (\hat{b}_{i,\mathcal{L}}^\dagger \hat{b}_{i,\mathcal{R}} + \text{H.c.}) - t_2 \sum_i (\hat{b}_{i,\mathcal{R}}^\dagger \hat{b}_{i+1,\mathcal{L}} + \text{H.c.}), \quad (2)$$

where t_1 is the intrawell hopping parameter between the left and right wells of a single double well on each site and t_2 is the interwell hopping parameter between adjacent left and right wells of double wells next to each other.

$$\hat{H}_U = \frac{U}{2} \sum_{\sigma=\mathcal{L},\mathcal{R}} \hat{n}_{i,\sigma} (\hat{n}_{i,\sigma} - 1) \quad (3)$$

is the on-site interaction on each site in both wells, and

$$\hat{H}_{U_{\mathcal{L}\mathcal{R}}} = U_{\mathcal{L}\mathcal{R}} \sum_i \hat{n}_{i,\mathcal{L}} \hat{n}_{i,\mathcal{R}} \quad (4)$$

defines the intrawell repulsion between bosons located in different wells on the same site. The repulsive interaction between neighboring sites is given by

$$\hat{H}_V = V \sum_{\sigma,\sigma'=\mathcal{L},\mathcal{R}} \hat{n}_{i,\sigma} \hat{n}_{i+1,\sigma'} \equiv V \sum_i \hat{n}_i \hat{n}_{i+1}. \quad (5)$$

Here we assume that the spatial distance between neighboring sites is much larger than the distance between the left and right wells of the double well on one site and therefore that V is independent of the well index σ . To abbreviate the notation, we define $\hat{n}_i = \hat{n}_{i,\mathcal{L}} + \hat{n}_{i,\mathcal{R}}$ and can omit most of the σ indices in the Hamiltonians.

The chemical potential term is

$$\hat{H}_\mu = -\mu \sum_{\sigma=\mathcal{L},\mathcal{R}} \hat{n}_{i,\sigma} \equiv -\mu \sum_i \hat{n}_i, \quad (6)$$

with the total boson number operator $\hat{N} = \sum_i \hat{n}_i$. The last Hamiltonian,

$$\begin{aligned} \hat{H}_{U_d} &= -\frac{U_d}{L} \left(\sum_{\substack{i \text{ even} \\ \sigma=\mathcal{L},\mathcal{R}}} \hat{n}_{i,\sigma} - \sum_{\substack{i \text{ odd} \\ \sigma=\mathcal{L},\mathcal{R}}} \hat{n}_{i,\sigma} \right)^2 \\ &= -\frac{U_d}{L} \left(\sum_{i \text{ even}} \hat{n}_i - \sum_{i \text{ odd}} \hat{n}_i \right)^2, \end{aligned} \quad (7)$$

represents the cavity-mediated long-range interaction between even and odd chain sites.

Hamiltonian (1) is identical to a dimerized chain with

$$\hat{H}_{\text{dim}} = -t \sum_j [1 + (-1)^{j+1} \delta] (\hat{b}_j^\dagger \hat{b}_{j+1} + \text{H.c.}), \quad (8)$$

where $t = (t_1 + t_2)/2$ is the mean hopping strength and $\delta = (t_1 - t_2)/(t_1 + t_2)$ is the bond dimerization. Likewise, the intrawell repulsion can be understood as a dimerized nearest-neighbor interaction,

$$\hat{H}_{U_{\mathcal{L}\mathcal{R}}, \text{dim}} = -\frac{U_{\mathcal{L}\mathcal{R}}}{2} \sum_j [1 + (-1)^{j+1}] \hat{n}_j \hat{n}_{j+1}. \quad (9)$$

The index j is here the combination of the i, σ notation into one index, where $j \equiv i, \mathcal{L}$ and $j + 1 \equiv i, \mathcal{R}$. Therefore, the chain length is doubled.

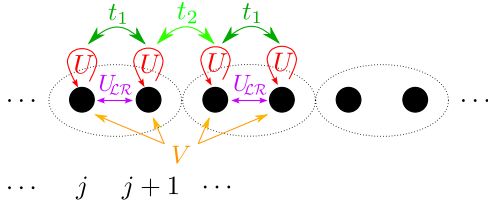


FIG. 2. Sketch of the dimerized chain described by Eq. (1). The \hat{H}_{U_d} term is not depicted. The dotted circles around two sites are a guide to the eye and correspond to the double wells in Fig. 1. The indices i, \mathcal{L} (i, \mathcal{R}) match j ($j+1$) and result in a dimerized chain length that is twice as long as the double-well chain.

Figure 2 represents Hamiltonian (1) in the form of a dimerized chain BHM, where the depicted interactions correspond to Fig. 1. The cavity-mediated long-range interaction is not shown. Each double well is equal to a pair of sites in the dimerized chain, highlighted by the dotted circle around the pair. Therefore, even and odd sites of the double-well BHM are an even and odd *pair of sites* of the dimerized chain, which is important to note for the cavity-mediated long-range interaction and the definition of the notation of the phases used in this work.

The intrawell repulsion acts as a dimerized interaction itself and can be regarded, for instance, as an interchain nearest-neighbor interaction of a two-leg ladder model [64]; however, the alignment of the sites is different between this model and the double-well Bose-Hubbard chain used in this work.

B. Simulation method and order parameters

We use the exact QMC worm algorithm (WA) [25,26] to obtain the phase diagrams. This method operates in the grand-canonical ensemble; thus, the boson number is not fixed. We consider chain lengths up to $L = 64$, where each site consists of one double-well potential. We elaborate the QMC-WA further in the Appendix.

From the QMC-WA simulations we obtain the boson density

$$\rho = \frac{1}{L} \sum_i \langle \hat{n}_i \rangle \quad (10)$$

and the superfluid density

$$\rho_s = \frac{\langle W^2 \rangle L}{2t_2\beta}, \quad (11)$$

with W being the winding number, which is defined as the difference between boson lines crossing the periodic boundary condition in one direction versus the other direction. For the relation between superfluid density and winding number in world-line QMC, see [21].

Furthermore with the density-density correlation $D(r) = \frac{1}{L} \sum_i \langle \hat{n}_i \hat{n}_{i+r} \rangle$, the structure factor is defined as

$$S(k) = \frac{1}{L} \sum_r e^{ikr} D(r). \quad (12)$$

TABLE I. Order parameters for the phases studied in this paper. We differentiate between (dimerized) MI and DW phases with even (e) and odd (o) particle numbers per double well.

	ρ_s	$S(\pi)$	$\mathcal{O}_s(\frac{L}{2})$	$\mathcal{O}_p(\frac{L}{2})$	ζ	Δ
SF	$\neq 0$	0	0	0	$\neq 0$	$\neq 0$
SS	$\neq 0$	$\neq 0$	$\neq 0$	$\neq 0$	$\neq 0$	$\neq 0$
DW($X_o, 0$)	0	$\neq 0$	$\neq 0$	$\neq 0$	0	1/2
DW($X_e, 0$)	0	$\neq 0$	$\neq 0$	$\neq 0$	0	0
MI(X_o)	0	0	0	$\neq 0$	0	1
MI(X_e)	0	0	0	$\neq 0$	0	0
HI(1)	0	0	$\neq 0$	0	0	$\neq 0$
D-DW($X_o, 0$)	0	$\neq 0$	$\neq 0$	$\neq 0$	$\neq 0$	$\neq 0$
D-DW($X_e, 0$)	0	$\neq 0$	$\neq 0$	$\neq 0$	$\neq 0$	$\neq 0$
D-MI(X_o)	0	0	0	$\neq 0$	$\neq 0$	$\neq 0$
D-MI(X_e)	0	0	0	$\neq 0$	$\neq 0$	$\neq 0$
D-HI(1)	0	0	$\neq 0$	0	$\neq 0$	$\neq 0$

With these order parameters we are able to distinguish between the MI, SF, DW, and SS phases. As shown in the single-well BHM with nearest-neighbor interactions, the so-called Haldane-insulator phase can emerge at the tip of the DW lobes [16,20], originating from the spin-1 antiferromagnetic Heisenberg chain [17,18]. To determine the HI we must introduce two nonlocal observables, the string and parity operators,

$$\mathcal{O}_s(|i-j|) = \left\langle \delta \hat{n}_i \exp \left\{ i\pi \sum_{k=i}^j \delta \hat{n}_k \right\} \delta \hat{n}_j \right\rangle, \quad (13)$$

$$\mathcal{O}_p(|i-j|) = \left\langle \exp \left\{ i\pi \sum_{k=i}^j \delta \hat{n}_k \right\} \right\rangle, \quad (14)$$

where $\delta \hat{n}_i = \hat{n}_i - \rho$ is the difference between the particle number and density. Due to periodic boundary conditions, both observables are evaluated for $|i-j| = L/2$.

Up until the HI(1) phase of Table I shows the phases which can be identified in the ground-state phase diagram with the help of the above-mentioned order parameters. As notation, we use for Mott-insulator phases MI(X), where X is the number of bosons in each double well. For the density-wave phases we use DW(X, Y), with X being the boson number on even sites and Y being the boson number on odd sites.

To further differentiate the behavior of the double-well dynamics, we introduce the intrawell fluctuation parameter

$$\zeta \propto \langle \hat{b}_{i,\mathcal{L}} \hat{b}_{i,\mathcal{R}}^\dagger + \text{H.c.} \rangle \quad (15)$$

as an indicator of the bosonic movement inside a double well between the left and right wells. It is linked to the kinetic-energy operator for dimerized models [59]. Furthermore, we define the well occupation difference

$$\Delta = \frac{1}{L} \sum_i \langle |\hat{n}_{i,\mathcal{L}} - \hat{n}_{i,\mathcal{R}}| \rangle. \quad (16)$$

When $\Delta = 0$, the boson distribution inside a double well is symmetric, meaning that as many particles are present in the left well as in the right well for every site. If $\Delta > 0$, the

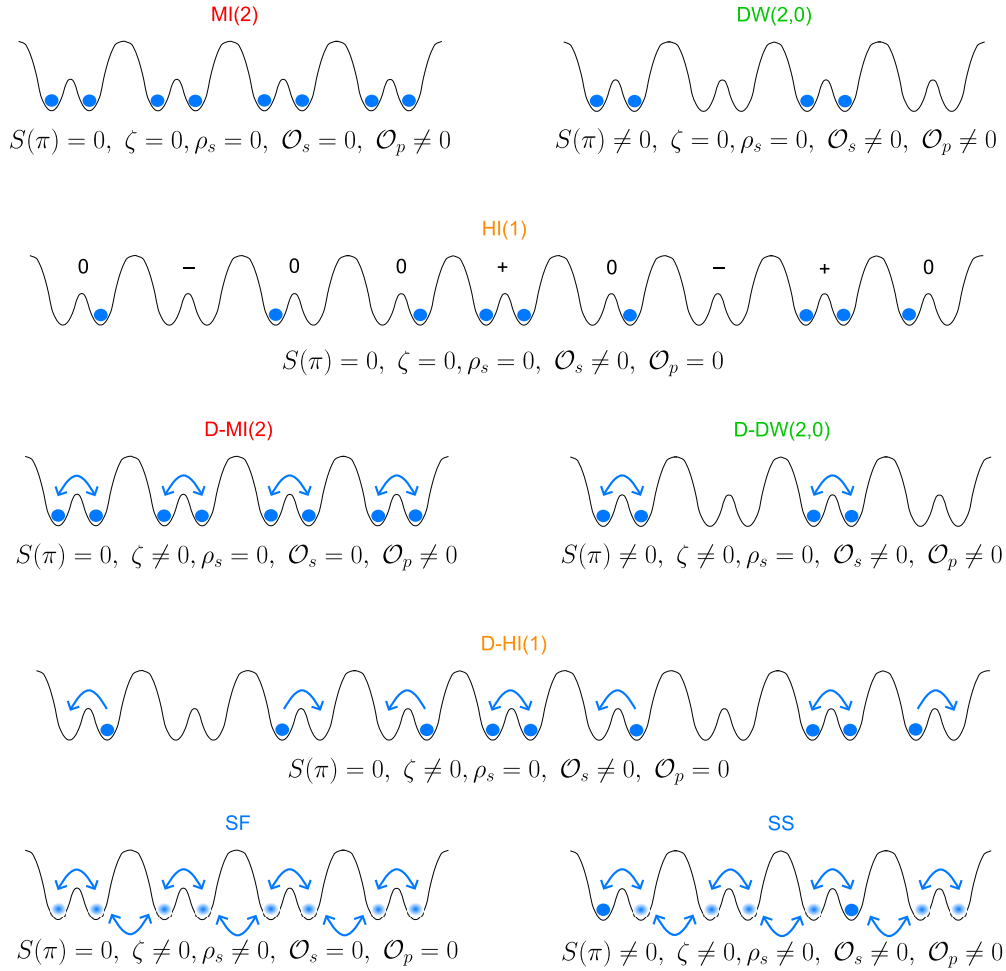


FIG. 3. Schematic representation of the phases in the double-well BHM. Localized bosons are depicted as blue saturated circles. In the case of the SF phase, all boson wave functions adopt one ground state and are delocalized. The blue blurred circles indicate the presence of delocalized bosons in the lattice, which are not bound to one position. In the SS phase, delocalized bosons are present on top of a localized density-wave structure. For the HI phase an additional representation of the occupation per site is given with the triplet $\{-, 0, +\}$. It shows the deviation from the mean particle number per site $\rho = 1$. The structure factor $S(\pi)$ is used to differentiate between MI and DW phases, while the intrawell fluctuation ζ indicates, for vanishing superfluid density ρ_s , dimerized phases. When $\rho_s \neq 0$, either a SF or SS phase is present, depending on the structure factor.

symmetry is (partially) broken, which happens when intrawell fluctuations become stronger. When $\zeta = 0$, all fluctuations inside the double wells vanish. For $\zeta > 0$ and $\rho_s = 0$ the movement inside the double wells can be compared to the dimerized BHM, where the finite bond dimerization leads to dimerized-Mott-insulator (D-MI), dimerized-density-wave (D-DW), and dimerized-Haldane-insulator (D-HI) phases [59]. The bottom part of Table I shows the dimerized phases, which are characterized by ζ and Δ .

In the following, we express all parameters in units of the on-site repulsion by the abbreviated form $\tilde{\mu} = \mu/U$, with analogous notation for all other parameters.

C. Ground states of the double-well BHM

The characteristic features of the phases defined in Table I are sketched in Fig. 3. In the SF phase, all bosons are delocalized, and the $U(1)$ symmetry is broken, while in the MI phase,

bosons localize uniformly on each site, and a particle-hole energy gap exists [1]. When the site occupation is restricted to 0, 1, and 2 and the density is fixed to 1, the BHM and Heisenberg chain are similar [20]. For the Heisenberg chain an underlying nonlocal discrete $\mathbb{Z}_2 \times \mathbb{Z}_2$ symmetry for the phases is associated [65]. While the HI phase breaks both \mathbb{Z}_2 symmetries, resulting in a nonvanishing string operator, in the MI phase the string operator vanishes. For the DW phase, the string operator is nonvanishing, but the structure factor is nonzero as well [66].

The intrawell fluctuation parameter describes the movement of bosons inside the double wells, while the superfluid density is related to the hopping of bosons along the double-well chain, in particular the hopping of bosons between sites. Hence, when the intrawell fluctuation parameter is nonzero but the superfluid density remains zero, a dimerization inside the double-well potentials occurs. When the superfluid density is nonzero, either a SF or SS phase is present. In the first case,

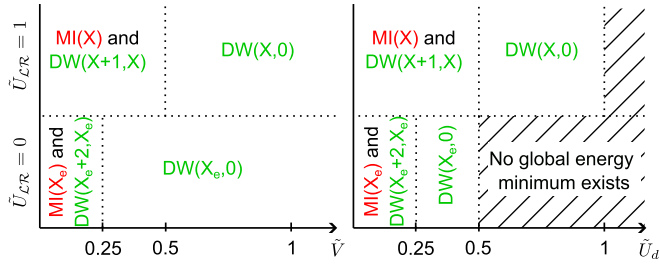


FIG. 4. Ground-state sketch of Hamiltonian (1) without hopping terms ($t_1 = t_2 = 0$) for $\tilde{V} > 0$, $\tilde{U}_d = 0$ (left) and $\tilde{V} = 0$, $\tilde{U}_d > 0$ (right) in the two cases $\tilde{U}_{\mathcal{LR}} = 0$ and $\tilde{U}_{\mathcal{LR}} = 1$. X is an integer number, while X_e represents only even integer numbers. When $\tilde{V} = 0$ and $\tilde{U}_d = 0$, DW phases vanish, and only MI phases persist.

all bosons are delocalized, while in the latter a long-range density order exists next to the superfluidity.

The structure factor $S(\pi)$ is used to distinguish between MI and DW as well as SF and SS phases. A nonzero superfluid density ρ_s determines whether a SF or SS phase is present. If the intrawell fluctuation is nonzero while the superfluid density remains zero, a dimerization of the phases occurs. The string and parity operators are used to differentiate the HI phase from the MI and DW phases.

The ground-state phase diagram of Hamiltonian (1) can be calculated analytically when the hopping terms are neglected because the number operator is diagonal in the Fock basis. In analogy to the ground-state phase diagrams of the single-well BHM and dimerized BHM we expect MI phases and DW phases to appear.

We do not differentiate between various boson configurations inside each double well. This is determined by the ratio of on-site repulsion and intrawell repulsion $U_{\mathcal{LR}}/U = \tilde{U}_{\mathcal{LR}}$. If $\tilde{U}_{\mathcal{LR}} < 1$, the symmetric filling of the left and right wells on each site is most favorable, and in the case of odd boson numbers, the last particle can be located in either well, resulting in two equally likely configurations for each double-well site.

In the case with $\tilde{U}_{\mathcal{LR}} = 1$, on-site repulsion and intrawell repulsion are equally strong. Thus, the energy gain from increasing the boson number in one well by one and the energy gain from increasing the boson number in the neighboring well on one site are the same. As a result, all boson distributions inside the double well share the same energy, and the degeneracy can be determined by combinatorics. To distribute X bosons in two wells, there are $\binom{X+2-1}{X} = X+1$ possible arrangements per site.

Figure 4 shows the ground-state phase diagram of the double-well BHM with cavity-mediated long-range interaction U_d and nearest-neighbor interaction V for $\tilde{U}_{\mathcal{LR}} = 0$ and $\tilde{U}_{\mathcal{LR}} = 1$.

Generally, nearest-neighbor and cavity-mediated long-range interactions have a lot of commonalities in their ground-state behavior, like on a mean-field level, where they show identical phase diagrams [38]. For $\tilde{U}_{\mathcal{LR}} = 0$, the occupation of the left and right wells on each site is symmetric; thus, only even particle numbers per site occur. One difference is the behavior when the interaction becomes sufficiently large compared to the on-site repulsion because for the cavity-

mediated long-range interaction there is no global energy minimum and thus no ground state anymore. One can see the reason for this in the energy per site which the system gains via the nearest-neighbor interaction and the long-range interaction,

$$\begin{aligned} \epsilon_V &= 4VXY, \\ \epsilon_{U_d} &= -\frac{U_d}{4}(X^2 + Y^2 - 2XY), \end{aligned} \quad (17)$$

where X and Y give the particle numbers on even and odd sites. Apparently, the nearest-neighbor interaction increases the energy when neighboring sites are occupied. This includes the MI phases, while DW phases remain unaffected. The reverse is true for the long-range interaction, where the energy decreases when an imbalance of particle occupation between even and odd sites is present, like for the DW phases, while the MI phases are unaffected by the long-range interaction. Hence, when the energy decrease from the long-range interaction is more than the energy gain from the on-site repulsion, the global energy function becomes a concave function, and no energy minimum exists anymore.

We can also explain why the transition points for $\tilde{U}_{\mathcal{LR}} = 0$ are halved compared to $\tilde{U}_{\mathcal{LR}} = 1$, as seen in Fig. 4. For $\tilde{U}_{\mathcal{LR}} = 0$, the Hamiltonian (1) without hopping terms scales by a factor of 2 in its on-site repulsion per site, while the nearest-neighbor and cavity-mediated long-range interactions both scale by a factor of 4 per site. On the other hand, for the $\tilde{U}_{\mathcal{LR}} = 1$ case, we first rewrite the on-site repulsion term (3) as

$$\hat{H}_U = \frac{U}{2} \sum_i \hat{n}_i(\hat{n}_i - 1) - U \sum_i \hat{n}_{i,\mathcal{L}} \hat{n}_{i,\mathcal{R}} \quad (18)$$

and see that the intrawell repulsion (4) and last term in Eq. (18) cancel each other out. What remains is the Hamiltonian of a single-well BHM, in which on-site repulsion and nearest-neighbor and cavity-mediated long-range interactions scale equally.

III. RESULTS

With the QMC-WA, we study the double-well BHM with inter- and intrawell hopping terms to analyze the ground-state phase diagrams for various parameter settings. We start with a brief summary of our key findings.

First, we discuss the ground states of the standard double-well BHM (without cavity-mediated long-range and nearest-neighbor interactions). We are interested in whether the dimerization of hopping terms results in dimerized MI and DW phases with noninteger densities, as expected from the dimerized chain [51,57]. Our results show the existence of dimerized MI phases with noninteger density. We furthermore study the D-MI(1) phase in detail for several dimerization strengths and its effects on the widths of the D-MI(1) lobe.

Next, we study the influence of the nearest-neighbor and long-range interactions. Of special interest for us is the $\rho = 1$ lobe. In the one-dimensional single-well BHM, a HI phase occurs at the tip of this lobe when a nearest-neighbor interaction is present, while a MI phase appears for cavity-mediated long-range interactions [42]. For the double-well

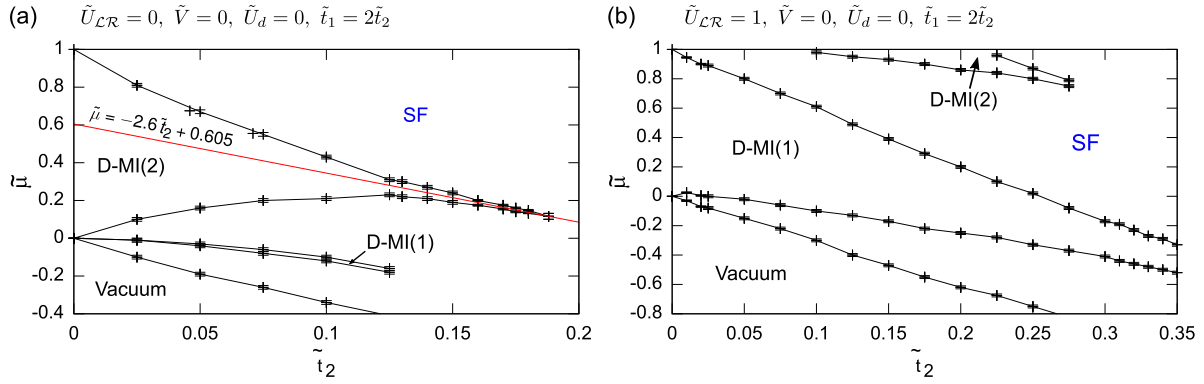


FIG. 5. Phase diagram of the standard double-well BHM with $\tilde{V} = \tilde{U}_d = 0$ and $\tilde{t}_1 = 2\tilde{t}_2$ for (a) $\tilde{U}_{\mathcal{LR}} = 0$ and (b) $\tilde{U}_{\mathcal{LR}} = 1$. For $\tilde{t}_2 = 0$, only MI phases are present in both cases, as discussed in Sec. II C. (a) When $\tilde{t}_2 > 0$, SF phases emerge between vacuum and D-MI phases, where D-MI phases replace the MI phases. A small D-MI(1) emerges between vacuum and the D-MI(2) phase. The tip of the D-MI(2) lobe is estimated to be around $\tilde{t}_2 \approx 0.22$ with the help of the analysis of the order parameters along the constant-particle-density line $\tilde{\mu} = -2.6\tilde{t}_2 + 0.605$. (b) When $\tilde{t}_2 > 0$, the D-MI phases persist for lower values of $\tilde{\mu}$ and stronger hopping strengths until the transition into SF phases compared to the $\tilde{U}_{\mathcal{LR}} = 0$ case. This indicates a stabilizing effect of the intrawell hopping for all D-MI(X) phases.

BHM we show that its phase diagram is qualitatively similar to that for the single-well BHM when the strengths of the intrawell potential and of the on-site repulsion are equal for both the nearest-neighbor and cavity-mediated interactions. For vanishing intrawell repulsion it turns out that noninteger-density D-DW phases also exist for soft-core bosons with nearest-neighbor interactions, which correspond to third-nearest-neighbor interactions in the dimerized BHM, and cavity-mediated long-range interactions.

Finally, we show that the intrawell hopping does not affect the existence of dimerized HI phases in the nearest-neighbor interaction case (independent of the intrawell potential), while for the double-well BHM with cavity-mediated long-range interactions and vanishing intrawell potential, the intrawell hopping suppresses a MI or HI phase at the tip of the $\rho = 1$ lobe.

A. Standard double-well BHM

The standard double-well BHM without intrasite repulsion $\tilde{U}_{\mathcal{LR}} = 0$ can be interpreted as a single-well dimerized BHM with double chain length (see Fig. 2). Then, the hopping terms correspond to the dimerized BHM via $t_1 = t + \delta$ and $t_2 = t - \delta$, with t being the mean hopping strength and δ being the dimerization factor. Therefore, the phase diagram of this parameter setting is expected to be identical to the phase diagram of the dimerized single-well BHM, where D-MI phases emerge, which are a combination of MI and bond-ordered phases [51,57,59]. The latter appear due to the broken translational symmetry of the dimerized model and are characterized by the alternating strengths of the bond kinetic energy [63].

The phase diagram is depicted in Fig. 5(a) and shows the expected behavior. For $\tilde{t}_2 > 0$ the MI phases are replaced by D-MI phases, where bosons move between the left and right wells of the sites. The D-MI(2) phase is identical to the D-MI(1) phase of a single-well dimerized BHM. We calculate the order parameters under the constant-density line $\tilde{\mu} = -2.6\tilde{t}_2 + 0.605$ to analyze the phase transition at

the tip of the lobe and show the results in Fig. 6. For $\rho_s = 0$, the D-MI(2) phase is present, while the transition to the SF phase takes place at around $\tilde{t}_2 \approx 0.22$, where the superfluid density becomes nonzero and independent of the system size. We compare the phase-transition point of our grand-canonical method to the canonical density-matrix renormalization-group technique used in [59], where the transition point is located around $\tilde{t}_2 \approx 0.23$, and can confirm that our results match the single-well dimerized BHM.

This agreement includes the fact that for any dimerization, $\delta \neq 0$, the MI phases are replaced by D-MI phases. The replacement to dimerized phases is also true for the DW and HI phases, which become D-DW and D-HI phases, respectively. The reason is the higher energy of the intrawell hopping compared to the interwell hopping. Fluctuations inside the double wells are more favorable than those between neighboring sites, which leads to different kinetic-energy contributions

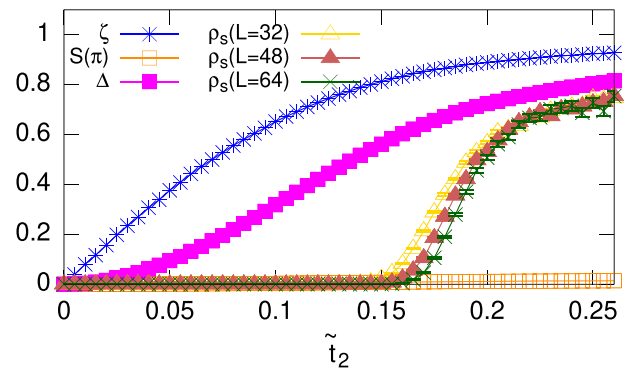


FIG. 6. Intrawell fluctuation ζ , structure factor $S(\pi)$, intrawell occupation difference Δ , and superfluid density ρ_s order parameters along the $\tilde{\mu} = -2.6\tilde{t}_2 + 0.605$ line with constant particle density $\rho = 2$ for different chain lengths. While $\rho_s = 0$, D-MI(2) is present. The tip of the lobe can be approximated by the position, where the superfluid densities of the different chain lengths overlap at $\tilde{t}_2 \approx 0.22$.

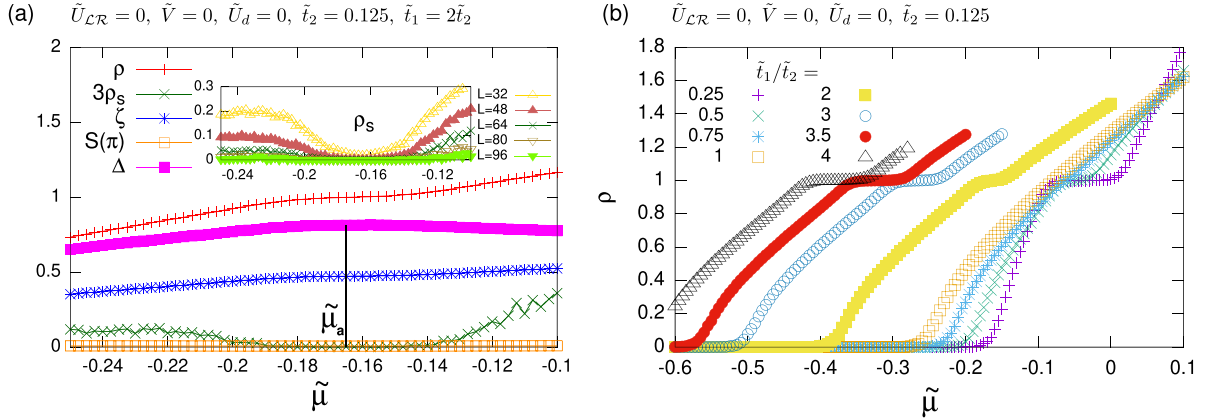


FIG. 7. (a) Density ρ , superfluid density ρ_s , intrawell fluctuation ζ , structure factor $S(\pi)$, and intrawell occupation difference Δ order parameters for $\tilde{t}_2 = 0.125$. The position $\tilde{\mu}_a \approx -0.165$ is a guide to the eye where Δ peaks. While ρ_s goes to zero, ζ remains monotonically increasing. In the inset the behavior of the superfluid density for increasing chain lengths is depicted, where a dip for $\rho = 1$ is visible and indicates the presence of the D-MI(1) phase. (b) The particle density ρ over the chemical potential $\tilde{\mu}$ for different ratios of \tilde{t}_1/\tilde{t}_2 . A plateau is formed for all dimerized hopping strengths and becomes broader the more the hopping strengths differ in size.

between the bond of the left and right wells in one double well and the bond between wells of neighboring sites.

The existence of a D-MI(1) phase in the standard double-well BHM with $\tilde{U}_{\mathcal{LR}} = 0$ is in accordance with the single-well BHM, in which no insulating phase exists, when the chain is not dimerized [28], but a MI-bond-order phase with $\rho = 1/2$ emerges when the chain is dimerized [51,57].

In Fig. 7, we investigate this phase in more detail. Beginning from the vacuum state, when the chemical potential is increased, bosons start to occupy the empty chain and can move inside the system via intrawell hopping (between the left and right wells of each double well on each site) or interwell hopping (between the left and right wells of double wells of neighboring sites). Approaching $\rho = 1$, nearly all double wells are occupied by one boson, and the well occupation difference Δ is maximized, as seen at $\tilde{\mu}_a$ in Fig. 7(a). As a result, when a boson hops to a double well of a neighboring site where another boson is already localized, it hinders the intrawell movement of that boson and cannot hop inside the new double well itself. This is energetically unfavorable, so the interwell hopping is suppressed. This effect will be overcome and the double-well chain will populate further with bosons only when the chemical potential becomes stronger. In the inset of Fig. 7(a) one can see the chain-length dependence of the superfluid order parameter, underlining the interwell hopping decrease around $\rho = 1$. Increasing the ratio \tilde{t}_1/\tilde{t}_2 enhances the aforementioned effect even further, and the D-MI(1) phase becomes bigger, as depicted in Fig. 7(b). When $\tilde{t}_1/\tilde{t}_2 < 1$, there is a plateau as well, although the intrawell hopping is weaker than the interwell hopping. This is no surprise, as a negative bond dimerization δ changes only the alternating order of the dimerized chain [Eq. (8)]. The shift of the density with respect to $\tilde{\mu}$ is explainable due to the change in the mean hopping strength.

For $\tilde{U}_{\mathcal{LR}} = 1$, the energy of a boson being in the same well as another one is equivalent to a boson being located in the neighboring well on the same site. Hence, the movement of a boson inside a double well is dependent solely on the intrawell

hopping parameter \tilde{t}_1 and not on the arrangement of bosons inside the double well. Figure 5(b) shows the phase diagram for the double-well BHM with $\tilde{U}_{\mathcal{LR}} = 1$ and $\tilde{t}_1 = 2\tilde{t}_2$.

The resemblance to the single-well BHM [28] is evident, as each double well in the double-well BHM for intrawell repulsion strength $\tilde{U}_{\mathcal{LR}} = 1$ behaves similarly in most ways to a single well. The important exception is the intrawell hopping \tilde{t}_1 , which introduces more energy due to the movement of bosons inside the double well and thus leads to a shift of the D-MI phases in the phase diagram to lower $\tilde{\mu}$ values and higher hopping values compared to the single-well BHM phase diagram, where $\tilde{t} = \frac{3}{2}\tilde{t}_2$.

B. Double-well BHM with nearest-neighbor and long-range interactions

We study the nearest-neighbor and cavity-mediated long-range interactions for different parameter settings and show the phase diagrams in Fig. 8. We have chosen the nearest-neighbor and long-range interaction strengths to be in the regime where, for $\tilde{t}_2 = 0$, only DW phases are present (see Fig. 4). We compare our results with the standard double-well BHM and the (dimerized) single-well BHM. For the nearest-neighbor interaction, at the tip of the DW(2,0) lobe a HI phase is found in the undimerized case [29], and a D-HI is found in the dimerized BHM [61]. For the single-well BHM with cavity-mediated long-range interaction a MI phase is located at the tip of the DW(2,0) lobe [42].

Regarding all phase diagrams presented in Fig. 8, when the hopping is greater than zero, MI, DW, and HI phases will become dimerized phases, meaning that bosons are localized in the double well on one site and fluctuate between the left and right wells of this double-well.

For $\tilde{U}_{\mathcal{LR}} = 0$, D-DW(X_o , 0) phases emerge between integer density phases for nearest-neighbor [Fig. 8(a)] and long-range [Fig. 8(c)] interactions. The reason for this is analogous to the D-MI(1) phase in the standard double well BHM in Fig. 5(a). Additionally, the D-DW phases are carried out for

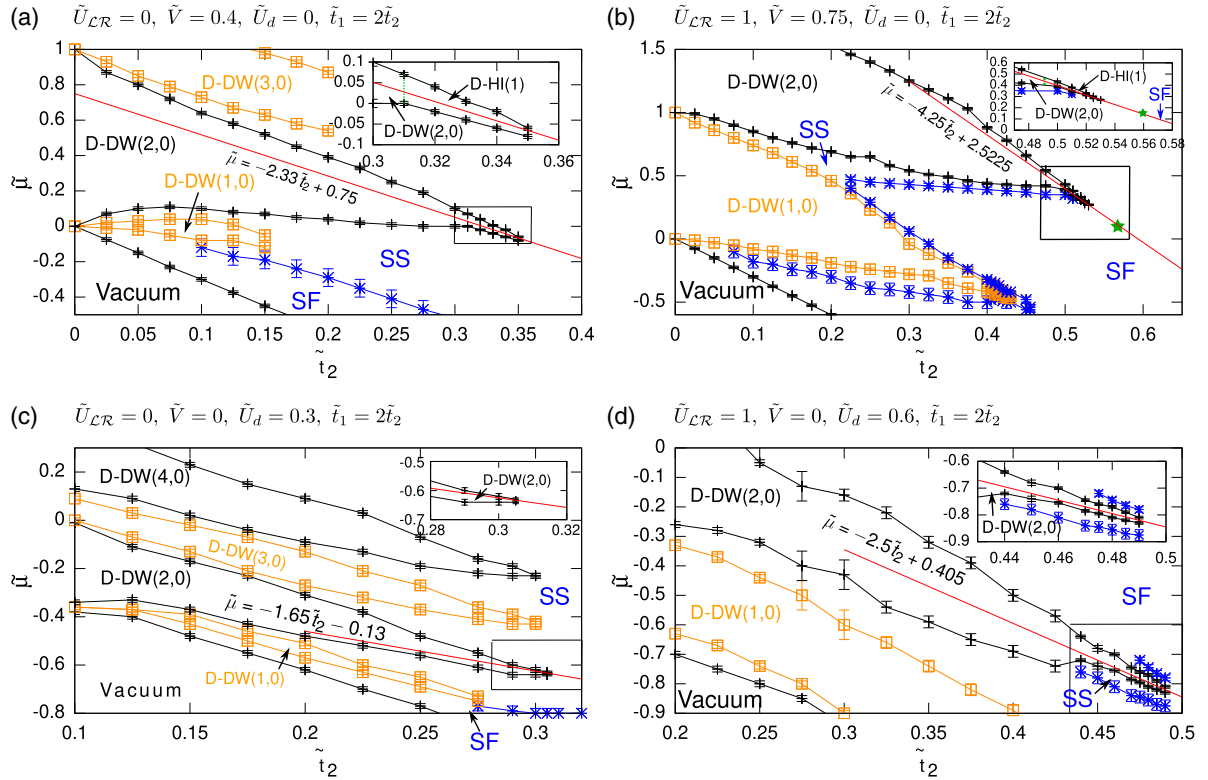


FIG. 8. Phase diagrams of the double-well BHM for (a) $\{\tilde{U}_{LR} = 0, \tilde{V} = 0.4, \tilde{U}_d = 0\}$, (b) $\{1, 0.75, 0\}$, (c) $\{0, 0, 0.3\}$, and (d) $\{1, 0, 0.6\}$ and $\tilde{t}_1 = 2\tilde{t}_2$. For $\tilde{t}_2 = 0$, only DW phases are present. Phases with noninteger densities are colored orange to better distinguish between the phases, and the tips of the D-DW(2, 0) lobes, where $\rho = 1$, are enhanced in the inset for all phase diagrams. The detailed behavior of the order parameters at the tip for constant densities is carried out along the red lines in Fig. 9. (a) When $\tilde{t}_2 > 0$, D-DW($X_e, 0$) phases with odd particle numbers per site X_e appear between D-DW($X_e, 0$) phases with even particle numbers. The transition between the SF phase and the SS phase is depicted via the blue line and is expected to engulf the D-DW(1,0) phase completely, so no direct transition from the SF to D-DW phase exists. The transitions from SS phases to SF phases for higher values of $\tilde{\mu}$ lie at higher hopping values than presented here. At the tip of the D-DW(2,0) phase a D-HI(1) phase is present. (b) When $\tilde{t}_2 > 0$, D-DW($X, 0$) phases emerge and are completely surrounded by SS phases. The transition between the SF phase and SS phase is depicted via the blue line. The transitions from SS phases to SF phases for higher values of $\tilde{\mu}$ are not presented here. A D-HI(1) phase appears at the tip of the D-DW(2,0) lobe, and a transition from D-HI(1) to SF can be determined at the position of the green star. (c) D-DW($X_e, 0$) phases, where X_e is even, appear as soon as hopping is included. In between, D-DW($X_o, 0$) phases, with X_o being odd, emerge due to the stabilizing effect of the intrawell hopping. The transition from the SF to SS phase is depicted via the blue line and is expected to engulf the D-DW(1,0) phase. Transitions from SS to SF phases for higher values of $\tilde{\mu}$ are not presented here. (d) D-DW($X, 0$) phases appear when the hopping terms are included. The D-DW phases are surrounded by a narrow SS phase, but only the transition at the tip is depicted via the blue line. At the tip of the D-DW(2,0) phase a transition to a D-MI(1) phase can be seen.

bigger hopping values. When $\tilde{V} > 0$, the SF and SS phases are shifted to higher energy values, while the D-DW phases are unaffected by the nearest-neighbor term and thus persist longer as in the standard double-well BHM. For the long-range interaction, when $\tilde{U}_d > 0$, the argumentation reverses. The energy of the D-DW phases decreases, while the SF and SS phases are unaffected. Hence, the D-DW phases persist not only for bigger hopping terms but also for smaller values of $\tilde{\mu}$.

For $\tilde{U}_{LR} = 1$, the argumentation that D-DW phases are present at higher hopping strengths and shift to lower $\tilde{\mu}$ values for the long-range interaction compared to the $\tilde{U}_{LR} = 0$ case remains the same for the phase diagrams with nearest-neighbor [Fig. 8(b)] and long-range [Fig. 8(d)] interactions. However, in contrast to the $\tilde{U}_{LR} = 0$ case, the D-DW($X_o, 0$) phases become broader when they approach $\tilde{t}_2 = 0$.

For the extended double-well BHM [Figs. 8(a) and 8(b)], at the tip of the D-DW(2,0) phase, a D-HI(1) phase can be identified, while for the long-range interaction [Figs. 8(c) and 8(d)] only at the tip of the D-DW(2,0) lobe for the $\tilde{U}_{LR} = 1, \tilde{U}_d = 0.6$ diagram can a D-MI(1) phase be extrapolated.

Figures 9(a)–9(d) show the order parameters along the constant-density lines of the corresponding phase diagrams in Figs. 8(a)–8(d). For small hopping values \tilde{t}_2 , the D-DW(2,0) phase is present in all panels of Fig. 9, where the superfluid density ρ_s is zero and all other parameters have nonzero values.

For the extended double-well BHM in Figs. 9(a) and 9(b) the D-DW(2,0) phase transitions into a D-HI(1) phase, where the structure factor $S(\pi)$ and parity order parameter \mathcal{O}_p drop to zero, while the string order parameter \mathcal{O}_s remains nonzero. The superfluid density becomes nonzero but is size

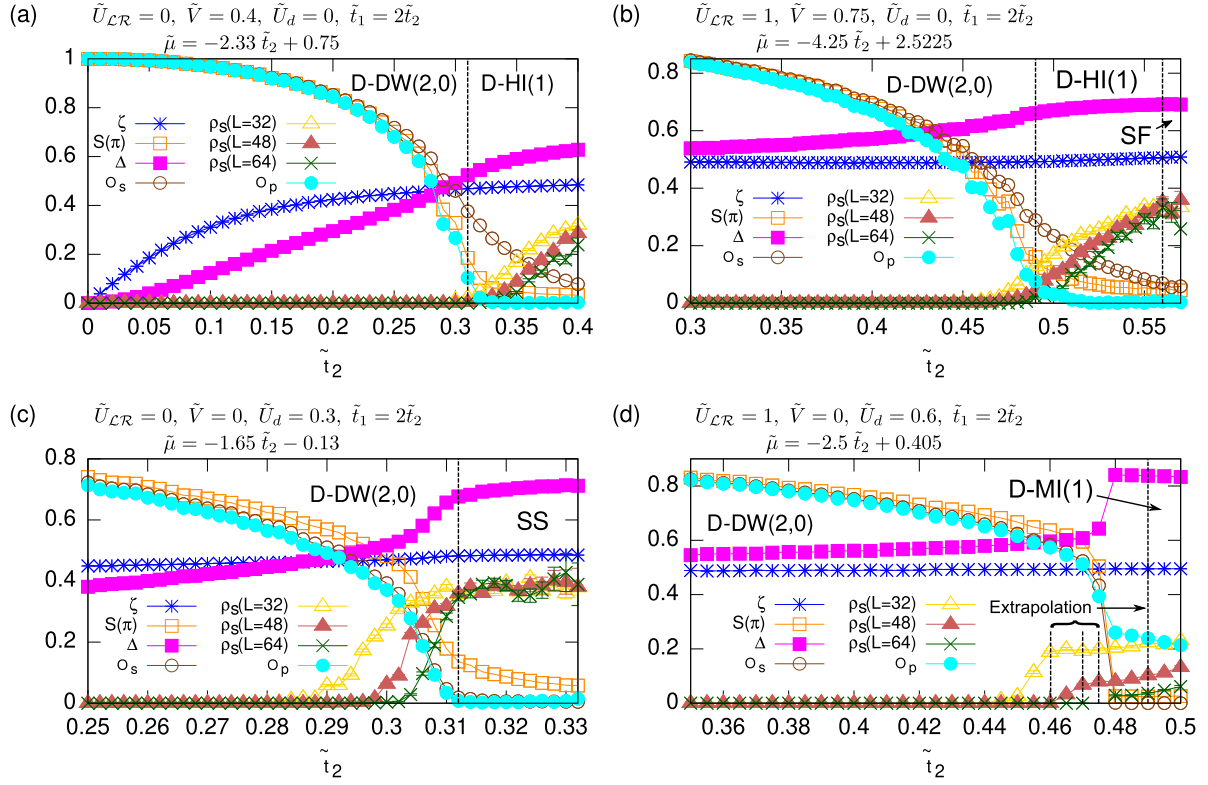


FIG. 9. Intrawell fluctuation ζ , structure factor $S(\pi)$, intrawell occupation difference Δ , superfluid density ρ_s , and string \mathcal{O}_s and parity \mathcal{O}_p order parameters along the constant-density ($\rho = 1$) lines (a) $\tilde{\mu} = -2.33 \tilde{t}_2 + 0.75$ for $\{\tilde{U}_{\mathcal{LR}} = 0, \tilde{V} = 0.4, \tilde{U}_d = 0\}$, (b) $\tilde{\mu} = -4.25 \tilde{t}_2 + 2.5225$ for $\{1, 0.75, 0\}$, (c) $\tilde{\mu} = -1.65 \tilde{t}_2 - 0.13$ for $\{0, 0, 0.3\}$, and (d) $\tilde{\mu} = -2.5 \tilde{t}_2 + 0.405$ for $\{1, 0, 0.6\}$ and $\tilde{t}_1 = 2\tilde{t}_2$. In the D-DW(2,0) phase, only the superfluid density is zero, while all other order parameters are nonzero. (a) At the transition point to the D-HI(1) phase at around $\tilde{t}_2 \approx 0.31$, $S(\pi)$ and \mathcal{O}_p vanish, while \mathcal{O}_s keeps a finite value. The superfluid density ρ_s attains nonzero values but approaches zero for larger chain lengths. (b) At the transition point to the D-HI(1) phase at around $\tilde{t}_2 \approx 0.49$, $S(\pi)$ and \mathcal{O}_p vanish, while \mathcal{O}_s keeps a finite value. The superfluid density ρ_s attains nonzero values but approaches zero for larger chain lengths. The transition to the superfluid phase can be determined at $\tilde{t} = 0.56$ when ρ_s becomes size independent and \mathcal{O}_s vanishes. (c) At the transition point $\tilde{t}_2 \approx 0.312$ the SS phase appears, as \mathcal{O}_s and \mathcal{O}_p vanish, while $S(\pi)$ remains present. No dimerized HI or MI phase can be identified between the D-DW(2,0) and SS phases. (d) At the transition point $\tilde{t}_2 \approx 0.49$ a D-MI(1) phase appears, as \mathcal{O}_s and $S(\pi)$ vanish, while \mathcal{O}_s remains present and ρ_s approaches zero for larger chain lengths. Because the point where the superfluid density becomes nonzero is highly dependent on the system size, we extrapolated it for the different sizes to obtain a better approximation of the transition point to the D-MI(1) phase.

dependent and becomes zero in the limit $L \rightarrow \infty$. Furthermore, in Fig. 9(b) the transition to the SF can also be seen, where ρ_s is size independent and nonzero, while \mathcal{O}_s approaches zero. Comparing these results for the D-HI phase with the results for the single-well extended BHM [29,42] shows that the topological HI phase persists in the double-well BHM in a dimerized way, in which the intrawell hopping does not break the long-range order of the HI phase.

Since the nearest-neighbor interaction of our double-well BHM is identical to the dimerized chain where the nearest-neighbor interaction acts on neighboring pairs of sites, we showed that the D-HI phase also persists for the dimerized chain with interactions up to the third neighboring site. This is an expansion of the results of Sugimoto *et al.* [61], in which a D-HI phase was found in the dimerized chain with nearest-neighbor interaction.

For the cavity-mediated long-range interaction with $\tilde{U}_{\mathcal{LR}} = 0$, $\tilde{U}_d = 0.3$, shown in Fig. 9(c), the D-DW(2,0) directly transits into the SS phase, where ρ_s and $S(\pi)$ are

nonzero and \mathcal{O}_s and \mathcal{O}_p are zero. To understand why no D-MI(1) phase exists at the tip of the D-DW(2,0) lobe, in contrast to the single-well BHM, in which a MI phase is present at the tip of the DW(2,0) lobe, we reiterate why the MI(1) phase exists in the single-well BHM in the first place.

The MI(1) phase appears at the tip of the DW(2,0) lobe in the single-well BHM because the intersite particle fluctuation per site scales in the MI phase by the power of U_d/L , as particles are evenly distributed between even and odd sites. On the other hand, intersite particle fluctuation per site for the DW(X, 0) phases scales by the factor $X^2 U_d/4$, making it independent of system size. This argumentation also holds true for the double-well BHM but is expanded by the effect of the intrawell hopping, in which the bosons in the D-DW(2,0) phase are able to fluctuate inside every second double well. This overcomes the effects of the cavity-mediated long-range interaction on the interwell fluctuations for the D-DW(2,0) phase and results in the D-DW(2,0) being present until the hopping strengths are strong enough that a direct transition into the SS phase occurs.

For the $\tilde{U}_{\mathcal{LR}} = 1$, $\tilde{U}_d = 0.6$ case, shown in Fig. 9(d), a transition to the D-MI(1) phase can be seen, where \mathcal{O}_p persists while ρ_s goes to zero for larger system sizes. Due to the strong variance of the starting point, where the superfluid density becomes nonzero according to system size, an extrapolation was carried out to determine the position of the transition to the D-MI(1) phase. The occurrence of a D-MI(1) at the tip of the D-DW(2,0) lobe in the double-well BHM with long-range interaction $\tilde{U}_d = 0.6$ matches the finding of a MI(1) phase at the tip of the DW(2,0) lobe in the single-well BHM with cavity-mediated long-range interaction [42]. This is reasonable, as we showed in Sec. II C for the double-well BHM without hopping that the double-well BHM with $\tilde{U}_{\mathcal{LR}} = 1$ is identical to a single-well BHM. Our results confirm that a dimerization of the hopping keeps the structure of a MI(1) phase at the tip of DW(2,0) but dimerizes these phases to D-MI(1) and D-DW(2,0), respectively.

IV. CONCLUSION

Short- and long-range order plays a fundamental role in the critical behavior of ultracold bosons in a quantum gas; thus, the ground-state behavior of the double-well BHM was studied numerically for different interactions. Furthermore, the results were compared to resembling dimerized chain models.

The one-dimensional double-well BHM with nearest-neighbor and cavity-mediated long-range interactions includes a variety of well-established models, such as the single-well BHM and the dimerized BHM. When dimerization is present, dimerized-Mott-insulator, dimerized-density-wave, and dimerized-Haldane-insulator phases exist, characterized by a combination of a bond-ordered phase [63] and a MI, DW, and HI phase, respectively. It turns out that dimerized hopping stabilizes the D-DW phases with noninteger boson densities, in agreement with results from dimerized chains [51,57]. When the intrawell repulsion is as strong as the on-site repulsion per well, each double well can be treated as a single well. Hence, in this case, the ground-state phase diagram is identical to the single-well BHM [28], with the exception that the intrawell hopping leads to dimerized phases and a shift of the D-MI phases to lower chemical potentials and higher hopping values.

Interactions between particles in neighboring double-well potentials imply interactions up to the third neighbor in the corresponding dimerized BHM. For those a D-HI phase at the tip of the D-DW lobe with a particle density of 1 exists, which was previously reported for a dimerized chain with solely nearest-neighbor interaction [61]. For noninteger densities D-DW phases exist, as was recently shown for the dimerized Bose-Hubbard chain with nearest-neighbor interactions [58].

In the presence of cavity-mediated long-range interactions a D-MI phase appears at the tip of the D-DW lobe with a density of 1 when the intrawell repulsion is as strong as the on-site repulsion, which is in agreement with results for the single-well chain BHM [42]. This D-MI phase at the tip of the D-DW phase disappears when the intrawell repulsion vanishes. This is due to the intrawell hopping, which distinguishes the D-DW phase in the double-well BHM and the

DW phase of the single-well BHM. Moreover, D-DW phases exist for noninteger densities in the double-well BHM with cavity-mediated long-range interaction, which is reminiscent of the double-well BHM with nearest-neighbor interaction and underpins the equivalence of nearest-neighbor and cavity-mediated long-range interactions on a mean-field level [38].

APPENDIX: QUANTUM MONTE CARLO WORM ALGORITHM

In this Appendix we discuss the quantum Monte Carlo worm algorithm we used to obtain the phase diagram of Hamiltonian (1) in more detail. We split the Hamiltonian into an on-diagonal part $\hat{\mathcal{H}}_{\text{on}}$ and off-diagonal part $\hat{\mathcal{H}}_{\text{off}}$ with regard to the Fock-basis representation of the one-dimensional (1D) chain $|\mathbf{n}_i\rangle = |n_1 \cdots n_L\rangle_i$. Hence, $\hat{\mathcal{H}}_{\text{on}}|\mathbf{n}_i\rangle$ gives the on-diagonal energy value ϵ_i . With the inverse temperature β and the Dyson series, we can write the partition function as

$$\mathcal{Z}(\mathcal{C}) = \sum_{m=0}^{\infty} \sum_{\mathbf{n}_1 \cdots \mathbf{n}_m} e^{-\beta \epsilon_1} \int_0^{\beta} d\tau_m \cdots \int_0^{\tau_2} d\tau_1 \times (e^{\tau_m \epsilon_1} \hat{\mathcal{H}}_{\text{off}}^{\mathbf{n}_1 \mathbf{n}_m} e^{-\tau_m \epsilon_m}) \cdots (e^{\tau_1 \epsilon_2} \hat{\mathcal{H}}_{\text{off}}^{\mathbf{n}_2 \mathbf{n}_1} e^{-\tau_1 \epsilon_1}), \quad (\text{A1})$$

with $\hat{\mathcal{H}}_{\text{off}}^{\mathbf{n}_i \mathbf{n}_j} = \langle \mathbf{n}_i | \hat{\mathcal{H}}_{\text{off}} | \mathbf{n}_j \rangle$. The partition function is the sum over all possible configurations, where m denotes the number of vertices in the system, as it counts the number of $\hat{\mathcal{H}}_{\text{off}}$ terms. The imaginary-time dimension is in the range $[0, \beta]$ and is segmented by the vertices in different lengths τ_m . Additionally, the Fock states at the beginning and the end must be the same $|\mathbf{n}_0\rangle = |\mathbf{n}_m\rangle$.

Now, the worm is inserted by including a $\hat{b}_i^\dagger \mathbf{n}'_i \mathbf{n}_c(\tau_c) \hat{b}_i \mathbf{n}'_i \mathbf{n}_a(\tau_a)$ or $\hat{b}_i \mathbf{n}'_i \mathbf{n}_a(\tau_a) \hat{b}_i^\dagger \mathbf{n}'_i \mathbf{n}_c(\tau_c)$ pair at an arbitrary

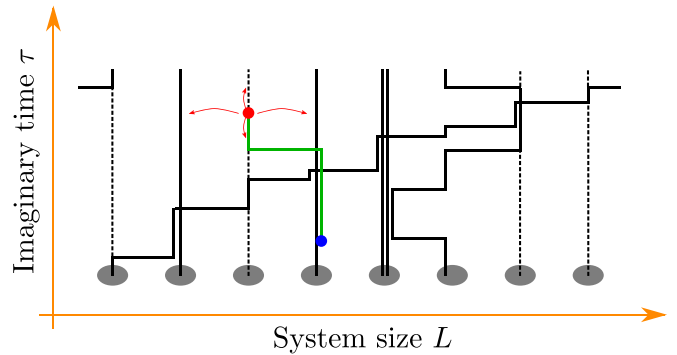


FIG. 10. Schematic movement of a worm inside the 1D chain. Solid black lines represent closed boson lines. Dashed black lines show vacancies. The open boson line is colored green and has the worm head (red) and tail (blue) as ends. The ends can move through the system as implied by the red arrows for the worm head. When head and tail collide, the worm closes, leaving new closed boson lines behind. Note that when at one site more than one boson is present, any of these bosons may perform a hopping, as they are all indistinguishable. The depiction here was chosen to easily see the occupation number per site. Also, the boson configuration at the start $\tau = 0$ must be the same as that at the end $\tau = \beta$.

site i and imaginary-time position $\tau_c = \tau_a$. In the first case, between the operators, a boson is removed, while in the second case a boson is created. Obviously, the worm is inserted only if a boson can be removed or the maximal number of bosons on one site is not surpassed when there is such a limit defined.

So the extended configuration for the partition function kernel reads

$$C^{\text{ext}} = \left(e^{\tau_m \epsilon_1} \hat{\mathcal{H}}_{\text{off}}^{\mathbf{n}_1 \mathbf{n}_m} e^{-\tau_m \epsilon_m} \right) \dots \left(e^{\tau_c \epsilon'_c} \hat{b}_i^{\dagger \mathbf{n}'_c \mathbf{n}_c} e^{-\tau_c \epsilon_c} \right) \dots \\ \times \left(e^{\tau_a \epsilon'_a} \hat{b}_i^{\mathbf{n}'_a \mathbf{n}_a} e^{-\tau_a \epsilon_a} \right) \dots \left(e^{\tau_1 \epsilon_2} \hat{\mathcal{H}}_{\text{off}}^{\mathbf{n}_2 \mathbf{n}_1} e^{-\tau_1 \epsilon_1} \right) \quad (\text{A2})$$

and vice versa for the other pairing. Without loss of generality we define the creator operator as the head and the annihilator operator as the tail. They can move through the configuration space by advancing forwards and backwards in imaginary time or by hopping according to the off-diagonal term $\hat{\mathcal{H}}_{\text{off}}$. When they come across an already existing vertex that they

cannot pass through (because the commutator does not vanish), one of three following scenarios occurs: (1) The vertex gets deleted, (2) the vertex is relinked to another site according to $\hat{\mathcal{H}}_{\text{off}}$, or (3) nothing happens, and the worm end moves in the other direction. The worm movement ends when the head and tail collide. Figure 10 sketches the 1D quantum chain, expanded with imaginary time to a classical two-dimensional model and the insertion of a worm.

With the QMC-WA it is possible to obtain grand-canonical and canonical observables. During worm movements the boson number is variable, allowing us directly to obtain the Green's function, for example. When the worm is deleted, the particle number is constant, and canonical observables can be calculated. The usual approach is via importance sampling,

$$\langle \mathcal{O} \rangle = \frac{1}{\mathcal{Z}} \sum_{\mathcal{C}} \mathcal{O}(\mathcal{C}) \mathcal{Z}(\mathcal{C}). \quad (\text{A3})$$

-
- [1] M. P. A. Fisher, P. B. Weichman, G. Grinstein, and D. S. Fisher, *Phys. Rev. B* **40**, 546 (1989).
- [2] D. Jaksch, C. Bruder, J. I. Cirac, C. W. Gardiner, and P. Zoller, *Phys. Rev. Lett.* **81**, 3108 (1998).
- [3] M. Greiner, O. Mandel, T. Esslinger, T. W. Hänsch, and I. Bloch, *Nature (London)* **415**, 39 (2002).
- [4] R. Landig, L. Hruby, N. Dogra, M. Landini, R. Mottl, T. Donner, and T. Esslinger, *Nature (London)* **532**, 476 (2016).
- [5] M. Anderlini, J. Sebby-Strabley, J. Kruse, J. V. Porto, and W. D. Phillips, *J. Phys. B* **39**, S199 (2006).
- [6] M. Anderlini, P. J. Lee, B. L. Brown, J. Sebby-Strabley, W. D. Phillips, and J. V. Porto, *Nature (London)* **448**, 452 (2007).
- [7] M. Atala, M. Aidelsburger, J. T. Barreiro, D. Abanin, T. Kitagawa, E. Demler, and I. Bloch, *Nat. Phys.* **9**, 795 (2013).
- [8] K. Baumann, C. Guerlin, F. Brennecke, and T. Esslinger, *Nature (London)* **464**, 1301 (2010).
- [9] E. Lieb, T. Schultz, and D. Mattis, *Ann. Phys. (NY)* **16**, 407 (1961).
- [10] J. B. Kogut, *Rev. Mod. Phys.* **51**, 659 (1979).
- [11] M. Ma, B. I. Halperin, and P. A. Lee, *Phys. Rev. B* **34**, 3136 (1986).
- [12] J. Tobochnik and G. V. Chester, *Phys. Rev. B* **20**, 3761 (1979).
- [13] D. C. Mattis, *Phys. Lett. A* **104**, 357 (1984).
- [14] J. M. Kosterlitz and D. J. Thouless, *J. Phys. C* **6**, 1181 (1973).
- [15] J. M. Kosterlitz, *J. Phys. C* **7**, 1046 (1974).
- [16] E. G. Dalla Torre, E. Berg, and E. Altman, *Phys. Rev. Lett.* **97**, 260401 (2006).
- [17] F. D. M. Haldane, *Phys. Rev. Lett.* **50**, 1153 (1983).
- [18] F. Haldane, *Phys. Lett. A* **93**, 464 (1983).
- [19] M. den Nijs and K. Rommelse, *Phys. Rev. B* **40**, 4709 (1989).
- [20] E. Berg, E. G. Dalla Torre, T. Giamarchi, and E. Altman, *Phys. Rev. B* **77**, 245119 (2008).
- [21] E. L. Pollock and D. M. Ceperley, *Phys. Rev. B* **36**, 8343 (1987).
- [22] D. M. Ceperley, *Rev. Mod. Phys.* **67**, 279 (1995).
- [23] G. G. Batrouni and R. T. Scalettar, *Phys. Rev. B* **46**, 9051 (1992).
- [24] G. G. Batrouni, R. T. Scalettar, G. T. Zimanyi, and A. P. Kampf, *Phys. Rev. Lett.* **74**, 2527 (1995).
- [25] N. Prokof'ev, B. Svistunov, and I. Tupitsyn, *Phys. Lett. A* **238**, 253 (1998).
- [26] N. V. Prokof'ev, B. V. Svistunov, and I. S. Tupitsyn, *J. Exp. Theor. Phys.* **87**, 310 (1998).
- [27] D. van Oosten, P. van der Straten, and H. T. C. Stoof, *Phys. Rev. A* **63**, 053601 (2001).
- [28] T. D. Kühner and H. Monien, *Phys. Rev. B* **58**, R14741 (1998).
- [29] G. G. Batrouni, R. T. Scalettar, V. G. Rousseau, and B. Grémaud, *Phys. Rev. Lett.* **110**, 265303 (2013).
- [30] T. Ohgoe, T. Suzuki, and N. Kawashima, *Phys. Rev. B* **86**, 054520 (2012).
- [31] P. Sengupta, L. P. Pryadko, F. Alet, M. Troyer, and G. Schmid, *Phys. Rev. Lett.* **94**, 207202 (2005).
- [32] G. G. Batrouni, F. Hébert, and R. T. Scalettar, *Phys. Rev. Lett.* **97**, 087209 (2006).
- [33] M. Iskin, *Phys. Rev. A* **83**, 051606(R) (2011).
- [34] D. Rossini and R. Fazio, *New J. Phys.* **14**, 065012 (2012).
- [35] K. Kawaki, Y. Kuno, and I. Ichinose, *Phys. Rev. B* **95**, 195101 (2017).
- [36] G. Schmid and M. Troyer, *Phys. Rev. Lett.* **93**, 067003 (2004).
- [37] Y.-C. Chen, R. G. Melko, S. Wessel, and Y.-J. Kao, *Phys. Rev. B* **77**, 014524 (2008).
- [38] N. Dogra, F. Brennecke, S. D. Huber, and T. Donner, *Phys. Rev. A* **94**, 023632 (2016).
- [39] T. Flottat, L. de Forges de Parny, F. Hébert, V. G. Rousseau, and G. G. Batrouni, *Phys. Rev. B* **95**, 144501 (2017).
- [40] L. Hruby, N. Dogra, M. Landini, T. Donner, and T. Esslinger, *Proc. Natl. Acad. Sci. USA* **115**, 3279 (2018).
- [41] B. Bogner, C. De Daniloff, and H. Rieger, *Eur. Phys. J. B* **92**, 111 (2019).
- [42] J. Sicks and H. Rieger, *Eur. Phys. J. B* **93**, 104 (2020).
- [43] V. Gurarie, L. Pollet, N. V. Prokof'ev, B. V. Svistunov, and M. Troyer, *Phys. Rev. B* **80**, 214519 (2009).
- [44] A. E. Niederle, G. Morigi, and H. Rieger, *Phys. Rev. A* **94**, 033607 (2016).
- [45] J. Sebby-Strabley, M. Anderlini, P. S. Jessen, and J. V. Porto, *Phys. Rev. A* **73**, 033605 (2006).

- [46] S. Fölling, S. Trotzky, P. Cheinet, M. Feld, R. Saers, A. Widera, T. Müller, and I. Bloch, *Nature (London)* **448**, 1029 (2007).
- [47] S. Trotzky, P. Cheinet, S. Fölling, M. Feld, U. Schnorrberger, A. M. Rey, A. Polkovnikov, E. A. Demler, M. D. Lukin, and I. Bloch, *Science* **319**, 295 (2008).
- [48] P. Barmettler, A. M. Rey, E. Demler, M. D. Lukin, I. Bloch, and V. Gritsev, *Phys. Rev. A* **78**, 012330 (2008).
- [49] X. Yin, L. Cao, and P. Schmelcher, *Europhys. Lett.* **110**, 26004 (2015).
- [50] A. G. Volosniev, D. Petrosyan, M. Valiente, D. V. Fedorov, A. S. Jensen, and N. T. Zinner, *Phys. Rev. A* **91**, 023620 (2015).
- [51] S. Mondal, S. Greschner, and T. Mishra, *Phys. Rev. A* **100**, 013627 (2019).
- [52] S. Peil, J. V. Porto, B. Laburthe Tolra, J. M. Obrecht, B. E. King, M. Subbotin, S. L. Rolston, and W. D. Phillips, *Phys. Rev. A* **67**, 051603(R) (2003).
- [53] G. K. Brennen, C. M. Caves, P. S. Jessen, and I. H. Deutsch, *Phys. Rev. Lett.* **82**, 1060 (1999).
- [54] B. Yang, H. Sun, C.-J. Huang, H.-Y. Wang, Y. Deng, H.-N. Dai, Z.-S. Yuan, and J.-W. Pan, *Science* **369**, 550 (2020).
- [55] P. J. Lee, M. Anderlini, B. L. Brown, J. Sebby-Strabley, W. D. Phillips, and J. V. Porto, *Phys. Rev. Lett.* **99**, 020402 (2007).
- [56] W. P. Su, J. R. Schrieffer, and A. J. Heeger, *Phys. Rev. Lett.* **42**, 1698 (1979).
- [57] F. Grusdt, M. Hönig, and M. Fleischhauer, *Phys. Rev. Lett.* **110**, 260405 (2013).
- [58] A. Hayashi, S. Mondal, T. Mishra, and B. P. Das, *Phys. Rev. A* **106**, 013313 (2022).
- [59] A. Kundu and S. K. Pati, *Europhys. Lett.* **85**, 43001 (2009).
- [60] M. Di Liberto, A. Recati, I. Carusotto, and C. Menotti, *Eur. Phys. J. Spec. Top.* **226**, 2751 (2017).
- [61] K. Sugimoto, S. Ejima, F. Lange, and H. Fehske, *Phys. Rev. A* **99**, 012122 (2019).
- [62] P. M. Azcona and C. A. Downing, *Sci. Rep.* **11**, 12540 (2021).
- [63] M. Nakamura, *J. Phys. Soc. Jpn.* **68**, 3123 (1999).
- [64] M. Singh, T. Mishra, R. V. Pai, and B. P. Das, *Phys. Rev. A* **90**, 013625 (2014).
- [65] T. Kennedy and H. Tasaki, *Phys. Rev. B* **45**, 304 (1992).
- [66] B. Grémaud and G. G. Batrouni, *Phys. Rev. B* **93**, 035108 (2016).